Spin-dependent pseudopotentials in the solid-state environment: Applications to ferromagnetic and antiferromagnetic metals

Vincent Cocula, Frank Starrost, Stuart C. Watson, and Emily A. Carter[a)]
Department of Chemistry and Biochemistry, University of California, Los Angeles, California 90095-1569

(Received 24 June 2003; accepted 23 July 2003)

The standard density-functional theory (DFT) pseudopotential method often fails to properly describe transition-metal-containing materials because the commonly used spin-averaged pseudopotentials fail to capture environment-dependent magnetic effects. Based on a perturbationlike theory, the spin-dependent pseudopotentials have been shown to accurately reproduce properties of transition metal atoms and bulk crystals within real space DFT formalisms. In the present paper, we revisit the question of the transferability of pseudopotentials for the study of transition elements and implement the spin-dependent pseudopotentials in the more standard approach to condensed matter DFT calculations—namely, the plane-wave pseudopotential DFT method. Applications to bulk Ni, Fe, and Cr and comparison with other pseudopotential methods show that the method promises to provide an enhancement of the pseudopotential transferability compared to the standard norm-conserving or ultrasoft pseudopotentials, even beyond the nonlinear core correction. © *2003 American Institute of Physics.* [DOI: 10.1063/1.1609399]

I. INTRODUCTION

Plane-wave-based density functional theories surely have become the methods of choice for studying condensed matter physics from first principles. They can be divided into all-electron (AE) and pseudopotential (PsP) theories. AE methods usually employ a mixed basis set, where the plane waves are augmented locally around each atomic site with radial solutions to the Schrödinger equation in order to accurately describe the oscillatory behavior of the wave function in the core region. The PsP method is an approximation to the AE method and is based on the well-known fact that the valence electrons are responsible for most chemical and physical properties of molecules and solids. It is therefore tempting to simplify the description of atoms to those of pseudoatoms, in which only the valence electrons are explicitly treated in the self-consistent calculation, thereby dramatically reducing the computational cost. Quantum mechanically, the electronic states of an atom are generally well separated energetically into discrete core and valence electronic states. It can be shown[1] that it is possible to create a new set of basis functions for the solution of the atomic Schrödinger equation so that one can calculate the valence states of the atom without explicitly taking the core electrons into account. These new functions are the so-called pseudo wave functions, which give rise to the so-called pseudopotential, which is a screened potential experienced only by the valence electrons. In order to ensure that the pseudo and AE wave functions and potentials are exactly identical in the valence region of the atom, both pseudo wave functions and pseudopotentials are set to match the AE wave functions and potentials beyond some core radius r_c.

The main advantage of the pseudopotential approach is its lower cost compared to AE methods. It is computationally far less demanding, and with the ever-increasing computational power available, it allows first-principles simulations of quite realistic and fairly large samples of condensed matter. The key to the reduced expense is that the pseudopotential replaces the true singular Coulombic potential by a much smoother one near the nucleus, and the pseudo wave functions are by construction smooth and nodeless within the core radius r_c. This is crucial when the electronic wave function is expanded in the usual solid-state basis of plane waves, as an enormous number of plane waves would be required to describe the oscillatory behavior of the AE valence wave function in the core region. Instead, by using pseudopotentials, a much smaller basis set is required to achieve basis set convergence. As a result, one always tries to make a pseudopotential as smooth as possible, thereby reducing the cost of the calculation while (hopefully) retaining the important physics. The quality of a pseudopotential is given by its transferability—i.e., its ability to produce results close to the AE ones when placed in different environments.

The theory and techniques for pseudopotential construction are well developed and have led to robust and efficient algorithms[2] for building accurate pseudopotentials. The construction of first-principles pseudopotentials has become a fairly routine procedure, where one chooses the atomic species to be pseudized, designates which electrons are to be kept as valence ones (sometimes explicitly keeping semicore electrons as well), and selects a level of theory for the solution of the atomic Kohn–Sham equations [e.g., the local density approximation (LDA) or flavors of the generalized gradient approximation (GGA)]. The AE equations are then solved for each angular momentum quantum number l in order to obtain the eigenenergies ε_l^{AE} and the set of AE wave

a)Author to whom correspondence should be addressed. Electronic mail: eac@chem.ucla.edu

functions ϕ_l^{AE}. For each angular momentum l, a core radius r_{cl} is chosen, usually equal to the outer maximum of the AE wave function, and a pseudo wave function ϕ_l^{ps} is constructed by smoothing out the AE one inside the radius r_{cl} and matching various derivatives of the wave function at r_{cl}. The Kohn–Sham equations are then iteratively inverted to solve for the pseudopotential v_l^{ps}, with the constraint that $\varepsilon_l^{ps}=\varepsilon_l^{AE}$.

Although the plane-wave pseudopotential method has proved to be accurate and reliable in many cases for the study of condensed phases, the method has been used sparingly for the study of open-shell transition-metal-based materials. Usually, the inaccuracies due to the PsP approximation are much smaller than other sources of error that density-functional theory (DFT) suffers from, among them the sensitivity of the method to the different choices of exchange-correlation potentials. By contrast, transition metals present a case of exception, whereby even within the same level of theory, a broad variety of results have been published for the exact same properties.[3] This is often indicative of variations in the pseudopotential choice and parametrization. The breakdown of the PsP approximation in the case of transition elements is due to their intrinsic physical properties. First, transition metals are open-shell systems, meaning that they can give rise to magnetism. Commonly, pseudopotentials are spin averaged so that they do not explicitly account for the variety of electronic spin states that may be adopted by the element. As a consequence, such spin-averaged pseudopotentials generally do a poor job at describing the magnetic properties of transition-metal-based materials. Second, they exhibit nearly degenerate ns and $(n-1)d$ electronic shells, making it difficult to separate the atom into core and valence states. A non-negligible overlap between core and valence densities exists; for accurate calculations, it is sometimes necessary to treat the semicore p electrons as valence states, which comes with a considerable (possibly prohibitive) computational cost as well. As a whole, the use of pseudopotentials is challenging for the study of transition elements. The problem is twofold: pseudopotential hardness and pseudopotential transferability.

A. Norm-conserving and ultrasoft pseudopotentials

One of the major steps in creating accurate and reliable pseudopotentials was the introduction of norm conservation[4] of the pseudo wave functions, which is necessary in order to accurately compute the exchange-correlation potential. This introduces an extra constraint for the construction of the pseudo wave function, and one usually requires that the norm of the AE and the pseudo wave function be exactly equal within the core region defined by $r<r_{cl}$. The resulting pseudopotential is then said to be ''norm conserving.'' One of the major problems in using norm-conserving pseudopotentials for transition metals in plane-wave-based methods is that the d wave function of those elements is very sharp and localized near the nucleus; indeed it has been shown[5] that it is impossible to construct a pseudo wave function much smoother than the AE one. Therefore one obtains a very sharp and localized pseudo wave function that requires a prohibitive number of plane waves to converge the basis set. Following the fix introduced by Rappe *et al.*,[6] one usually manually sets the cutoff radius r_{cd} to be much greater than the maximum of the AE d wave function, so that it is still possible to construct smooth enough pseudo wave functions for practical use in plane-wave codes. This is often not totally satisfactory, since one dramatically reduces the transferability of the pseudopotential by doing so. One often has to find the best compromise between transferability and hardness of the potential, but the study of transition metal materials using norm-conserving pseudopotentials still remains expensive if one wants to perform somewhat accurate calculations.

One way around this problem is to use the so-called Vanderbilt ''ultrasoft'' pseudopotentials. Vanderbilt showed[5] that by solving a generalized eigenvalue problem, one can relax the norm-conservation constraint and thus build accurate, reliable, and computationally inexpensive pseudopotentials. The cutoff radius r_{cl} for which the AE and pseudo wave function have to match is no longer necessarily set to be the outermost maximum of the wave function, but rather the cutoff is chosen so that it gives rise to an optimally smooth pseudo wave function. The pseudo wave function is no longer norm conserving in this case, and the deficit in valence electron density introduced by this relaxation is compensated for by an atom-centered augmentation charge function. It becomes then quite inexpensive to perform plane-wave calculations on transition metals, and it is sometimes stated that ultrasoft pseudopotentials are more reliable and transferable than norm-conserving ones.[7] But even if the first fact is obvious and of great importance (reducing the expense), it is rather unclear if ultrasoft potentials are really more accurate and transferable than norm-conserving ones. In fact, they have been shown in multiple instances to give qualitatively equivalent results.[8] We will discuss later several examples demonstrating that they do not seem to dramatically enhance the transferability of a potential. We would rather state that for comparable transferability, ultrasoft potentials have the great advantage of being inexpensive, even allowing one to treat explicitly the semicore p electrons as valence electrons, which is sometimes required for accurate calculations.

B. Nonlinear core correction

When one generates first-principles pseudopotentials, the Kohn–Sham equations[9] have to be solved for the atom, and one gets as output the total screened potential containing the sum of all three ionic, Hartree, and exchange-correlation potentials. One then has to remove the Hartree and exchange-correlation potentials to get the actual ionic pseudopotential to be used in the solid-state calculation. The Hartree and exchange-correlation contributions by the valence density will be added back in self-consistently in the plane-wave code, depending on the chemical environment in which the species are placed. Since only the contribution of the Hartree and exchange-correlation potentials due to the valence density is removed to unscreen the total potential, this implicitly assumes a linearization of those potentials with respect to its density dependence. It is well known that the exchange-correlation part is a nonlinear function of the density, while

TABLE I. Atomic energy splitting (AES) between the high-spin (spherically averaged) s^2d^6 and s^1d^7 states of Fe, as given by an all-electron (AE) and by several pseudopotential DFT-LSD calculations, using a NLCC with different values of the core radius r_c^{NLCC} (in Å). $\mathrm{AES}=E(s^1d^7)-E(s^2d^6)$.

	AE	$r_c^{\mathrm{NLCC}}=0.00$	0.10	0.40	0.70	0.85	1.10
AES (eV)	0.10	0.27	0.27	0.41	1.10	1.78	2.46

the Hartree potential is a linear function of the density. This implicit (and incorrect) linearization of the exchange-correlation potential introduces systematic inherent errors in a pseudopotential calculation, and the problem becomes even more dramatic in the case of transition elements where a non-negligible overlap between core and valence densities exists. The problem was first mentioned by Louie *et al.*,[10] who introduced the so-called nonlinear core correction (NLCC). Ultimately, one would like to use the full (including both core and valence charge densities) exchange-correlation potential to unscreen the total atomic potential, but this is impractical within a plane-wave basis because it would require a prohibitive number of plane waves in order to accurately describe the very sharp core charge density near the atomic sites. Instead, a function $\rho^c_{\mathrm{at,smooth}}(r)$ is used, which is constructed to recover the exact core charge density beyond some arbitrary NLCC core radius r_c^{NLCC}. The use of a NLCC can improve the transferability of a pseudopotential, but is not a totally satisfactory fix, because not only are the choices of the NLCC function and its associated core radius not uniquely defined, but the quality of the calculation is highly sensitive to those choices.[11] As an example, Table I shows the sensitivity to the choice of the NLCC core radius of a pseudopotential calculation of the atomic energy splitting between the high-spin (spherically averaged) s^2d^6 and s^1d^7 states of Fe. As we can see, the deviation between the AE and pseudopotential values grows dramatically as the cutoff radius r_c^{NLCC} increases. It is generally accepted that a reasonable compromise is to choose this cutoff equal to where core and valence densities have equal contributions, which corresponds in our case to $r_c^{\mathrm{NLCC}}=0.70$ Å. This dramatic sensitivity of energetics on the core radius choice was also observed and discussed in a recent paper,[11] in which the authors appear to claim that reducing the value of r_c^{NLCC} solves the inaccuracy problem. Once again, not only is this intractable within plane-wave-based methods, but also within the local spin density approximation (LSDA), it has been shown[12] that inherent errors of the exchange-correlation functional make it undesirable to use the full core charge density. We will see that even if the correction provided by a NLCC is of great importance, it cannot be regarded as the ultimate solution to increase the PsP transferability. The problems and complications that transition metal atoms pose to the pseudopotential approximation go largely beyond the nonlinearity of the exchange-correlation potential.

C. Spin-dependent pseudopotentials

The spin-dependent pseudopotentials (SD-PsPs) have been invented by Watson and Carter.[13] The main idea is to systematically correct the conventional spin-averaged pseudopotentials by accounting explicitly for the variable spin states adopted by the atom, ensuring a correct treatment of core spin polarization in relevant cases (e.g., transition metals). The whole theory is based on a perturbationlike approximation, where a reference spin-neutral pseudopotential is corrected by a polarization potential, modulated by the atomic local valence spin polarization. The pseudopotential is thus divided into two potentials, one for the spin-up case and one for the spin-down case.

For open-shell systems like transition metals, it is obvious that the atomic wave functions as well as their associated potentials will be distinct for up- and down-spin electrons. During the process of creating the pseudopotential, one usually performs a spin-polarized calculation to create up-spin and down-spin pseudo wave functions and potentials. Once this is done, one usually creates new spin-averaged potentials and wave functions by averaging the spin-up and spin-down functions weighted by the corresponding average electronic polarization. Then, after unscreening, this provides a unique spin-averaged, angular-momentum-dependent pseudopotential

$$v_l^{SA}(r)=\frac{N_e^{\uparrow}}{N_e}v_l^{\uparrow}(r)+\frac{N_e^{\downarrow}}{N_e}v_l^{\downarrow}(r), \tag{1}$$

where N_e is the total number of valence electrons (in the atomic case) and $N_e^{\uparrow}$ and $N_e^{\downarrow}$ the number of electrons with spin up and spin down, respectively. An alternative means to generate such a spin-averaged pseudopotential is simply to perform the atomic calculation on the nonmagnetic (spin-neutral) electronic configuration—i.e., where each shell of electrons is constrained to have an equal number of up and down spins.

For a spherically symmetric atom, the ion–electron interaction energy is given by

$$E^{\mathrm{ion}}=\int 4\pi r^2 v(r)n(r)dr, \tag{2}$$

where $n(r)$ is the valence charge density. In the Watson–Carter spin-dependent formalism, the potential is now not only angular momentum dependent, but also spin dependent. The total ionic energy is then the sum of the contribution of the up- and down-spin channels:

$$E^{\mathrm{ion}}=\int 4\pi r^2[v^{\uparrow}(r)n^{\uparrow}(r)+v^{\downarrow}(r)n^{\downarrow}(r)]dr, \tag{3}$$

where the up and down potentials are taken as the sum of the spin-neutral reference pseudopotential v^0 and of the "polarization potential" δv,

$$v^{\uparrow}(r)=v^0(r)+F[\beta(r)]\delta v(r),$$

TABLE II. Atomic energy splitting (AES) between the high-spin (spherically symmetric) s^2d^6 and s^1d^7 states of Fe, as given by an all-electron (AE) and by several pseudopotential DFT-LSDA calculations.

	AE	SN-PsP	SN-PsP+NLCC	SD-PsP	US-PsP	US-PsP+NLCC
AES (eV)	0.10	2.50	1.10	0.10	2.30	0.40

$$v^{\downarrow}(r)=v^{0}(r)+F[-\beta(r)]\delta v(r), \tag{4}$$

with a functional dependence $F[\beta(r)]$ through the local spin polarization $\beta(r)$:

$$\beta(r)=\frac{n^{\uparrow}(r)-n^{\downarrow}(r)}{n^{\uparrow}(r)+n^{\downarrow}(r)}. \tag{5}$$

In Eq. (4), the potential v^0 is the pseudopotential generated using the nonmagnetic (i.e., half-up-spin, half-down-spin) electronic configuration for the element of interest and δv represents the perturbative potential. This perturbative potential is essentially the difference between the potential constructed from the fully polarized (high-spin) electronic configuration (denoted v^{fp}) and the spin neutral one (denoted v^0), scaled by the atomic local spin polarization,

$$\delta v(r)=\frac{v^{\mathrm{fp}}(r)-v^{0}(r)}{\beta_{\mathrm{at}}(r)[2-\beta_{\mathrm{at}}(r)]}, \tag{6}$$

so that the new spin-dependent potentials are spin polarization dependent and will give rise therefore to a more or less perturbed potential depending on the local electronic configuration taken by the element studied in its particular environment. The functional form used in this work is the one suggested by Watson and Carter, where the functional F is simply taken as $F[\beta(r)]\equiv\beta(r)$. According to Eqs. (3)–(5), the expression for the potentials then becomes[13]

$$v^{\uparrow}(r)=\frac{\delta E^{\mathrm{ion}}}{\delta n^{\uparrow}(r)}=v^{0}(r)+\beta(r)[2-\beta(r)]\delta v(r),$$

$$v^{\downarrow}(r)=\frac{\delta E^{\mathrm{ion}}}{\delta n^{\downarrow}(r)}=v^{0}(r)-\beta(r)[2+\beta(r)]\delta v(r). \tag{7}$$

In their original work, Watson and Carter showed[13] that accounting for the spin dependence dramatically improves the transferability of a pseudopotential for the description of the atomic eigenvalues and energy splittings between two different polarized atomic states.

As an example of results from the different pseudopotential methods discussed previously, we show in Table II the energy splitting between the high-spin (spherically symmetric) s^2d^6 and s^1d^7 atomic states of Fe given by an AE DFT-LSDA calculation and several pseudopotential methods, including spin-neutral norm-conserving (SN-PsP) and ultrasoft (US-PsP) pseudopotentials, used with or without a nonlinear core correction (NLCC), and by a spin-dependent norm-conserving pseudopotential (SD-PsP). For the SN-PsP, we used a $r_c^{\mathrm{NLCC}}=0.70$ Å. This is a strong test of transferability of a pseudopotential and it is interesting to see that, as we discussed earlier, even if the great advantage of ultrasoft potentials is their rather inexpensive computational cost, it does not seem obvious at all that they provide necessarily more transferable pseudopotentials than norm-conserving ones. The general trend is that the inclusion of a NLCC systematically corrects this lack of transferability, for obvious reasons stated before, but we have shown that this fix is not necessarily satisfactory from a theoretical point of view. On the other hand, the spin-dependent pseudopotential gives an energy splitting in this case identical to the one found in an AE calculation, as Watson and Carter showed in their original paper. Those results for atoms tend to demonstrate that the spin-dependent pseudopotentials, being defined with no arbitrary extra parameters (e.g., as in a NLCC) have a great role to play in improving the quality of the DFT pseudopotential method for its use for transition-metal-based materials, and ensuing work has focused on implementing and applying the method to condensed phases of such elements.

Consequently, the spin-dependent pseudopotential method was implemented recently in the real-space DFT code HARES by Starrost *et al.*[14] and was shown again to give significant improvement of the transferability of pseudopotentials over the conventional spin-neutral ones for bulk transition metal crystals. The goal of our current work is to show that it is also possible (but not trivial) to implement the spin-dependent pseudopotentials into a reciprocal-space DFT method working with a plane-wave basis on a uniform Fourier grid. Given that most condensed matter electronic structure calculations are carried out using the latter approach, it is essential to outline such an implementation and to demonstrate its feasibility in order for the spin-dependent pseudopotentials to be employed more widely in the future.

II. IMPLEMENTATION DETAILS

As one can see from the formalism, Eq. (7) has to be implemented in real space, and it does not seem obvious at first how to implement the method in a reciprocal-space scheme, working with plane waves on a discrete uniform Fourier grid. We show in this section that it is still possible to use the spin-dependent pseudopotentials in reciprocal-space algorithms, since they are based on a dual representation between real and reciprocal spaces by means of fast Fourier transforms (FFTs).

The form of the pseudopotential used is the one of Kleinman and Bylander,[15] where the total potential is divided into local and nonlocal angular-momentum-dependent parts, so that the total ionic pseudopotential takes the form

$$v_{ps}=v_{\mathrm{local}}+\sum_{lm}\frac{|\Delta v_l\phi_l\rangle\langle\phi_l\Delta v_l|}{\langle\phi_l|\Delta v_l|\phi_l\rangle}, \tag{8}$$

where the Δv_l's are

$$\Delta v_l=v_l-v_{\mathrm{loc}} \tag{9}$$

and the ϕ_l's are the pseudo wave functions. In the spin-dependent formalism, the potential for each angular momentum l is given by

$$v_l^{\uparrow\downarrow} = v_l^0 \pm \beta(2 \mp \beta)\,\delta v_l, \tag{10}$$

which translates into a local and nonlocal description by

$$v_l^{\uparrow\downarrow} = v_{\mathrm{loc}}^0 \pm \beta(2 \mp \beta)\,\delta v_{\mathrm{loc}} + \Delta v_l^0 \pm \beta(2 \mp \beta)\,\delta\Delta v_l \tag{11}$$

for which the nonlocal contributions are taken as

$$\begin{aligned} \Delta v_l^0 &= v_l^0 - v_{\mathrm{loc}}^0, \\ \delta\Delta v_l &= \frac{\Delta v_l^{\mathrm{fp}} - \Delta v_l^0}{\beta_{\mathrm{at}}(2-\beta_{\mathrm{at}})}. \end{aligned} \tag{12}$$

The total spin-dependent pseudopotential in Kleinman–Bylander form thus becomes

$$v_{ps}^{\uparrow\downarrow} = v_{\mathrm{loc}}^0 \pm \beta(2 \mp \beta)\,\delta v_{\mathrm{loc}} + \sum_{lm} \frac{|[\Delta v_l^0 \pm \beta(2 \mp \beta)\,\delta\Delta v_l]\phi_l^0\rangle\langle\phi_l^0[\Delta v_l^0 \pm \beta(2 \mp \beta)\,\delta\Delta v_l]|}{\langle\phi_l^0|[\Delta v_l \pm \beta(2 \mp \beta)\,\delta\Delta v_l]|\phi_l^0\rangle}. \tag{13}$$

In Eq. (8), the conventional projectors $|\Delta v_l \phi_l\rangle\langle\phi_l \Delta v_l|$ as well as the scaling factors $\langle\phi_l|\Delta v_l|\phi_l\rangle$ are only atomic functions, independent of any quantity computed during the calculation itself. As we can see in Eq. (13), this is no longer the case in the spin-dependent potentials, where both the projectors and scaling factors possess an explicit dependence on the self-consistent charge density (through the spin polarization β). The major consequence of this is that both the projectors and scaling factors have to be built and evaluated at each iteration in the SCF cycle.

In the Kleinman–Bylander form, the local potential includes the long-ranged Coulombic part of the pseudopotential, while the nonlocal parts are essentially short-ranged corrections to it. It has been demonstrated[13] that most of the correction due to the spin-dependent potentials is short ranged and localized around each nucleus, so we would like to perturb only the nonlocal part of the total potential, noting also that the perturbation added does not include any Coulombic-like behavior. This is possible due to the flexibility of the Kleinman–Bylander form: for the reference state used to construct the pseudopotential, the choice of local and nonlocal parts is arbitrary, while of course orbital energies will be slightly changed for all other configurations. It is thus possible to alter the local potential by any arbitrary operator $\hat{A}$,[3] provided that one accounts for it in the nonlocal projectors, so that we have the identity

$$\begin{aligned} v_{ps} &= v_{\mathrm{loc}} + \sum_{lm} \frac{|\Delta v_l \phi_l\rangle\langle\phi_l \Delta v_l|}{\langle\phi_l|\Delta v_l|\phi_l\rangle} \\ &= v_{\mathrm{loc}} - \hat{A} + \sum_{lm} \frac{|(\Delta v_l + \hat{A})\phi_l\rangle\langle\phi_l(\Delta v_l + \hat{A})|}{\langle\phi_l|(\Delta v_l + \hat{A})|\phi_l\rangle}. \end{aligned} \tag{14}$$

This manipulation is of great importance for the spin-dependent potentials, and if we set an operator

$$\hat{A}^{\mathrm{sdp}} = \delta v_{\mathrm{loc}} = \frac{v_{\mathrm{loc}}^{\mathrm{fp}} - v_{\mathrm{loc}}^0}{\beta_{\mathrm{at}}(2-\beta_{\mathrm{at}})}, \tag{15}$$

then Eq. (13) simplifies into

$$v_{ps}^{\uparrow\downarrow} = v_{\mathrm{loc}}^0 + \sum_{lm} \frac{|\{\Delta v_l^0 \pm \beta(2 \mp \beta)[\,\delta\Delta v_l + \hat{A}^{\mathrm{sdp}}]\}\phi_l^0\rangle\langle\phi_l^0\{\Delta v_l^0 \pm \beta(2 \mp \beta)[\,\delta\Delta v_l + \hat{A}^{\mathrm{sdp}}]\}|}{\langle\phi_l^0|\{\Delta v_l \pm \beta(2 \mp \beta)[\,\delta\Delta v_l + \hat{A}^{\mathrm{sdp}}]\}|\phi_l^0\rangle} \tag{16}$$

such that only the nonlocal projectors have to be self-consistently updated.

The form of the potential in Eq. (16) is only defined within a given chemical environment [through the local spin-polarization $\beta(\mathbf{r})$]. We therefore cannot conduct the traditional logarithmic derivative transferability tests[16] on our new SD-PsP, but will judge instead its quality by its environment-dependent transferability. While the analysis of the logarithmic derivatives may be of some use when one wants to measure the transferability of a pseudopotential, it has been previously shown that such tests are not always enough, and environment-dependent tests are still of great importance.[17]

A. Generation procedure

Given a local spin polarization, the spin-dependent pseudopotential is completely defined by two potentials: the spin-neutral reference potential $v^0(r)$ and the perturbative part of the potential, $\delta v(r)$.

The spin-neutral reference potential is generated by using the classic scheme proposed by Troullier and Martins.[2] By ''spin-neutral'' we mean that we generate the pseudopotential for the nonmagnetic electronic configuration. For example, for iron (Fe), which has a ground-state valence electronic configuration of $4s^2 3d^6$, we will generate the pseudopotential for the spherically symmetric atom by using

the nonmagnetic configuration $4s^{1\uparrow,1\downarrow}3d^{3\uparrow,3\downarrow}$.

For the perturbation added to the spin-neutral potential, the procedure is a little bit more complex. As we saw, this perturbation has the form (for each angular momentum)

$$\delta v_l(r) = \frac{v_l^{\mathrm{fp}}(r) - v_l^0(r)}{\beta_{\mathrm{at}}(r)[2-\beta_{\mathrm{at}}(r)]}. \tag{17}$$

The perturbation δv_l added to the spin-neutral potential requires the generation of a second pseudopotential $v^{\mathrm{fp}}(r)$, which is the potential affecting the majority spin for the fully polarized electronic configuration of the element studied. For the example of Fe, this corresponds to the spherically symmetric $4s^{1\uparrow,1\downarrow}3d^{5\uparrow,1\downarrow}$ electronic configuration. After carrying out the spin-polarized atomic calculation, one only keeps the potential affecting the majority-spin channel and, from the corresponding pseudo wave functions $\phi_l^{\mathrm{fp}}(r)$, computes the atomic local spin polarization $\beta_{\mathrm{at}}(r)$.

Traditionally, a set of fractions α_s, α_p, and α_d of the s, p, and d potentials to be used as the local part of the potential is chosen so that

$$\begin{aligned} v_{\mathrm{loc}}^0 &= \alpha_s v_s^0 + \alpha_p v_p^0 + \alpha_d v_d^0, \\ v_{\mathrm{loc}}^{\mathrm{fp}} &= \alpha_s v_s^{\mathrm{fp}} + \alpha_p v_p^{\mathrm{fp}} + \alpha_d v_d^{\mathrm{fp}}, \end{aligned} \tag{18}$$

where v_{loc}^0 is the reference spin-neutral local potential. The corresponding nonlocal contributions to be used in the Kleinman–Bylander form are the projectors

$$P_l^0 = |\Delta v_l^0 \phi_l^0\rangle, \tag{19}$$

with $\Delta v_l^0 = v_l^0 - v_{\mathrm{loc}}^0$. We then build the perturbation terms to be input for use in the self-consistent spin-dependent calculation, where the local part is expressed by the operator $\hat{A}^{\mathrm{sdp}}$ in Eq. (15), and the perturbation to the Kleinman–Bylander projectors are then taken as

$$\delta P_l = \left(\frac{\Delta v_l^{\mathrm{fp}} - \Delta v_l^0}{\beta_{\mathrm{at}}(2-\beta_{\mathrm{at}})} + \hat{A}^{\mathrm{sdp}} \right) \phi_l^0. \tag{20}$$

B. Nonlocal part: Projectors

The evaluation of the nonlocal energy in reciprocal space requires, prior to the calculation, the computation of the reciprocal-space representation of the Kleinman–Bylander projectors for each angular momentum considered, using the Bessel—Fourier transform

$$P_l(q) = \int_0^\infty 4\pi r^2 \Delta v_l \phi_l(r) j_l(qr) dr, \tag{21}$$

where the j_l's are Bessel functions of order l. The evaluation of the nonlocal potential energy is then atom dependent, and the contribution of the jth atom in the unit cell from band n and at the k point $\mathbf{k}$ is[18]

$$\epsilon_{\mathbf{k},n}^j = \sum_{lm} \xi_l^{-1} Z_{lm}^* Z_{lm}, \tag{22}$$

where

$$Z_{lm} = \sum_G \lambda_{lm}(\mathbf{G}+\mathbf{k}) c_{(\mathbf{G}+\mathbf{k}),n} \tag{23}$$

and

$$\lambda_{lm}(\mathbf{G}+\mathbf{k}) = \frac{4\pi i^l}{\sqrt{\Omega}} P_l(|\mathbf{G}+\mathbf{k}|) Y_{lm} e^{i(\mathbf{G}+\mathbf{k})\cdot\tau_i}, \tag{24}$$

where Ω is the volume of the primitive cell, ξ_l is an l-dependent energy (a scaling factor, defined below), τ_i is the position vector of the ith atom in the cell, and the $c_{(\mathbf{G}+\mathbf{k}),n}$'s are the plane-wave coefficients. The sum in Eq. (23) runs over all values of $|\mathbf{G}+\mathbf{k}|$ that are less than a maximum $\mathbf{G}$ vector, $\mathbf{G}_{\mathrm{max}}$, which is the plane-wave cutoff.

It has been shown that the evaluation of the nonlocal energy can also be done accurately in real space[18] and that this offers better scaling of the method when one studies large systems. Since the spin-dependent formalism is based on a real-space representation, naturally we prefer a real-space evaluation of the nonlocal energy. In a real-space formulation, Eq. (23) translates to

$$Z_{lm} = \int_{|\boldsymbol{r}-\boldsymbol{R}_\mu|<r_c} P_l(\boldsymbol{r}-\boldsymbol{R}_\mu) Y_{lm} \Psi_{\boldsymbol{k},n}(\boldsymbol{r}) d^3r, \tag{25}$$

where $\mathbf{R}_\mu$ is the position of atom μ in the cell. Because the projector functions $P_l(r)$ are short-ranged and vanish outside the sphere of radius r_c, this integration can be done in a time independent of the system size, thus reducing the burden of the reciprocal-space integration for large supercells. The main drawback of the real-space projection is that care must be employed if it is ever used for small supercells. The periodic boundary conditions can create spurious self-overlap of the projector functions if their range is longer than half the cell size.

The method we employ is the one of King-Smith, Payne, and Lin,[18] where they showed that the integration of Eq. (25) can be done on a uniform FFT grid of mesh vectors $\boldsymbol{\iota}$ by variationally computing a set of radial projection operators $\chi_l(r)$ adapted for the real-space grid, so that we finally have the identity

$$Z_{lm} = \Omega \sum_{\boldsymbol{\iota}} \chi_l(\boldsymbol{\iota}-\boldsymbol{R}_\mu) Y_{lm} \Psi_{\boldsymbol{k},n}(\boldsymbol{\iota}). \tag{26}$$

In order to evaluate the nonlocal energy in real space for the spin-dependent pseudopotential, both $\chi_l^0(r)$ and $\chi_l^{\mathrm{fp}}(r)$ are derived[18] from the corresponding projectors $P_l^0(q)$ and $\delta P_l(q)$ and the perturbation $\delta\chi_l(r)$ to the nonlocal potential is formed so that

$$\delta\chi_l(r) = \frac{\chi_l^{\mathrm{fp}}(r) - \chi_l^0(r)}{\beta(r)[2-\beta(r)]} + A^{\mathrm{sdp}}(r) \tag{27}$$

and the numerical integration thus becomes

$$\begin{aligned} Z_{lm}^{\uparrow\downarrow} = \Omega \sum_{\boldsymbol{\iota}} & [\chi_l(\boldsymbol{\iota}-\boldsymbol{R}_\mu) \pm \beta(\boldsymbol{\iota})[2 \mp \beta(\boldsymbol{\iota})] \\ & \times \delta\chi_l(\boldsymbol{\iota}-\boldsymbol{R}_\mu)] Y_{lm} \Psi_{\boldsymbol{k},n}(\boldsymbol{\iota}). \end{aligned} \tag{28}$$

C. Nonlocal part: Scaling factors

Since the spin dependence of the pseudopotential modifies the expression for the Kleinman–Bylander projectors (the nonlocal part of the pseudopotential), then for consis-

TABLE III. Atomic parameters used for the pseudopotential generation. See text for detailed explanations.

Element	XC type	Nonmagnetic configuration	r_c (bohr)			Local potential			r_c^{NLCC} (bohr) (if any)
			$r_{c,s}$	$r_{c,p}$	$r_{c,d}$	α_s	α_p	α_d	
Ni	LDA	$s^{1\uparrow,1\downarrow}d^{4\uparrow,4\downarrow}$	2.91	2.10	2.07	0.85	0.00	0.15	n/a
Fe	LDA	$s^{1\uparrow,1\downarrow}d^{3\uparrow,3\downarrow}$	2.26	3.05	2.00	0.90	0.00	0.10	1.11
Fe	PBE	$s^{1\uparrow,1\downarrow}d^{3\uparrow,3\downarrow}$	2.29	3.09	1.99	0.90	0.00	0.10	1.11
Cr	LDA	$s^{1/2\uparrow,1/2\downarrow}d^{5/2\uparrow,5/2\downarrow}$	2.58	3.61	1.80	0.85	0.00	0.15	1.54
Cr	PBE	$s^{1/2\uparrow,1/2\downarrow}d^{5/2\uparrow,5/2\downarrow}$	2.61	3.66	1.79	0.85	0.00	0.15	1.54

tency one needs to update also the Kleinman–Bylander scaling factors ξ_l's. As we saw in Eq. (8), in the spin-neutral formalism, this scaling factor is an atomic quantity, independent of any self-consistent quantity computed during the calculation. As a result, the scaling factors can be evaluated once for all before one starts the calculation, equal to the one-dimensional integral

$$\xi_l = \langle \phi_l | \Delta v_l | \phi_l \rangle = \int 4\pi r^2 \phi_l^* \Delta v_l \phi_l dr. \tag{29}$$

In the spin-dependent formalism, the situation is rather different. First, this scaling factor has to be updated self-consistently during the calculation because it now also depends on the local spin polarization β, as seen in Eq. (13). Second, since this local spin polarization is a three-dimensional object, the integration has to be done in the entire space spanned by the unit cell of the crystal studied. In fact, the total scaling factor can be rewritten as

$$\begin{aligned}\xi_l^{\mathrm{sdp}} &= \langle \phi_l^0 | \Delta v_l^0 \pm \beta(2 \mp \beta)[\delta \Delta v_l + \hat{A}^{\mathrm{sdp}}] | \phi_l^0 \rangle \\ &= \int \phi_l^{0*} (\Delta v_l^0 \pm \beta(2 \mp \beta)[\delta \Delta v_l + A^{\mathrm{sdp}}) \phi_l^0 d\mathbf{r} \\ &= \xi_l^0 \pm \int \phi_l^{0*} \beta(2 \mp \beta)[\delta \Delta v_l + A^{\mathrm{sdp}}] \phi_l^0 d\mathbf{r},\end{aligned} \tag{30}$$

where ξ_l^0 is the scaling factor of the spin-neutral reference potential, which is computed beforehand and is simply treated as a real number. Note that the ϕ_l^0's implicitly contain the spherical harmonics in addition to the radial part. We then are left with the evaluation (at each iteration) of the second term on the right-hand side of Eq. (30). This can be conveniently evaluated in reciprocal space if we define an atom-centered function

$$\mathcal{O}_l(r) = \phi_l^{0*}(r)[\delta \Delta v_l(r) + A^{\mathrm{sdp}}(r)] \phi_l^0(r) \tag{31}$$

and the three-dimensional function $f(\boldsymbol{r}) = \pm \beta(\boldsymbol{r})[2 \mp \beta(\boldsymbol{r})]$. The integral in the last line of Eq. (30) exactly equals the sum over their respective Fourier representations, so that

$$\int f(\boldsymbol{r}) \mathcal{O}_l(\boldsymbol{r} - \boldsymbol{R}_\mu) d^3 r = \Omega \sum_{\boldsymbol{G}} f(\boldsymbol{G}) S_\mu(\boldsymbol{G}) \mathcal{O}_l(\boldsymbol{G}), \tag{32}$$

where $\boldsymbol{R}_\mu$ is the position of atom μ and S_μ is an atomic structure factor.

III. CALCULATIONAL DETAILS

We have implemented our spin-dependent pseudopotential method in the plane-wave pseudopotential DFT code CASTEP.[19] We constructed norm-conserving pseudopotentials for Ni, Fe, and Cr, all generated using the Troullier–Martins scheme[2] using a high-accuracy atomic code originally developed by Froyen and modified by Troullier and Martins. Table III shows the atomic parameters used to generate our spin-neutral pseudopotentials. We generated two sets of PsPs for Fe and Cr, one for the LSD and the other for the PBE approximations of the exchange-correlation potential. Table III also gives the electronic configuration used to generate the spin-neutral reference pseudopotential; not shown are the fully polarized, high-spin, configurations with the same spherically averaged s- and d-shell occupancies that are used to build the perturbative part of the spin-dependent pseudopotential. The table displays also the cutoff radii r_c's for each angular momentum channel, the coefficients used to build the local part of the Kleinman–Bylander forms, and the cutoff radii r_c^{NLCC}'s used when a NLCC was applied. The ultrasoft potentials used for this study were the ones provided with the CASTEP package, version 4.2. When the NLCC was employed for our norm-conserving pseudopotentials, we used a polynomial expansion of the partial core density inside the cutoff radius r_c^{NLCC},

$$\rho_c^{\mathrm{NLCC}}(r) = \begin{cases} \rho_c(r) & \text{for } r > r_c^{\mathrm{NLCC}}, \\ \exp\left(\sum_{i=0}^{2} a_i r^{2i} \right) & \text{for } r \leqslant r_c^{\mathrm{NLCC}}, \end{cases} \tag{33}$$

where the value of the cutoff r_c^{NLCC} was chosen so that it corresponds to the point in space where core and valence charges are of equal magnitude. This produced smooth functions that did not require a larger basis, while at the same time allowing us to recover most of the overlapping core density so that using a smaller cutoff radius was unnecessary. All local spin density approximation (LSDA) calculations were performed using the spin-polarized Ceperley–Alder[20] exchange-correlation potential as parametrized by Perdew and Zunger;[21] for the gradient-corrected potentials, we used the PBE (Ref. 22) parametrization of the GGA. All calculations were converged with respect to the plane-wave basis and **k**-point sampling within the first Brillouin zone [a mesh of $10 \times 10 \times 10$ was used for all primitive body-centered-cubic (bcc, two atoms) cells, while a $8 \times 8 \times 8$ mesh was sufficient for conventional face-centered-cubic (fcc, four atoms) cells]. For theoretical consistency, we unscreened the pseudopotential with the same exchange-correlation potential as the one used for the self-consistent solid-state calculation. We note that the use of GGAs to unscreen the pseudopotential may be problematic in that the gradient of the density

TABLE IV. DFT-LSDA bulk properties of fcc Ni: lattice constant a_0, bulk modulus B_0, and magnetic moment per atom, M.

	a_0 (Å)	B_0 (GPa)	M (μ_B)
Experiment	3.52	184	0.62
FLAPW[a]	3.42	254	0.62
SN-PsP	3.51	227	0.78
SD-PsP	3.50	240	0.57
SN-PsP[b]	3.49	209	0.77
SD-PsP[c]	3.48	208	0.57
SN-PsP[d]	3.50	237	0.78

[a]Reference 23.
[b]Reference 14.
[c]Reference 14.
[d]Reference 24.

TABLE V. DFT-LSDA bulk properties of bcc Fe: lattice constant a_0, bulk modulus B_0, and magnetic moment per atom, M.

	NLCC	a_0 (Å)	B_0 (GPa)	M (μ_B)
Experiment	n/a	2.87	167	2.20
FLAPW[a]	n/a	2.75	250	1.98
SN-PsP	no	2.97	127	3.13
SD-PsP	no	2.81	254	2.00
US-PsP	no	2.90	168	3.18
SN-PsP	yes	2.83	229	2.15
SD-PsP	yes	2.83	240	2.13
US-PsP	yes	2.73	283	1.95

[a]Reference 23.

introduced by them generates undesirable wiggles in the potential near the nucleus. In this case, the use of a NLCC can be very helpful in smoothing out the potential, and in the case of the spin-dependent pseudopotential, we find it is a mandatory procedure. Since the perturbative part of the potential is essentially the difference between two potentials, those wiggles become a numerically undesirable feature. Therefore, all GGA calculations were performed using a NLCC.

Since the new potential is self-consistently updated, one might expect an increase in computational expense associated with its use. However, the overhead cost associated with the spin dependence turns out to be negligible when compared to the same spin-neutral calculation. Occasionally, a few extra iterations are required to achieve electronic convergence; however, there are also cases where it converges faster than the spin-neutral case.

IV. RESULTS

We present properties of Ni, Fe, and Cr bulk crystals, using both conventional spin-neutral and spin-dependent pseudopotential DFT. Those results are compared to AE DFT and other pseudopotential DFT calculations (mainly using US-PsPs). The goal of this study is to show the systematic improvement in the transferability of the pseudopotentials and of the treatment of magnetic phases when one uses the spin-dependent pseudopotentials. It is important to understand that the pseudopotential method is an approximation of the AE case, and so one should always judge the quality of a pseudopotential calculation by its ability to reproduce AE results rather than experimental values. With this goal in mind, we did not try to construct the best (most transferable) pseudopotentials possible. For future applications, it will be useful to adjust the pseudopotential parameters to optimize smoothness and transferability prior to their widespread use. Here, our interest is simply to gauge the systematic (or lack thereof) improvement due to the use of the spin-dependent pseudopotentials, regardless of the quality of the original spin-neutral pseudopotentials.

A. Bulk nickel

Table IV displays properties [the lattice constant (a_0), the bulk modulus (B_0), and the magnetic moment per atom (M)] of fcc Ni using a variety of approaches, all within DFT-LSDA. For completeness, we include the experimental values as well. We report previous AE full-potential linear-augmented plane-wave (FLAPW) results,[23] which serve as our benchmarks. Next we list our results for the spin-neutral pseudopotential (SN-PsP), for the spin-dependent pseudopotential (SD-PsP), and results obtained previously by Starrost *et al.*[14] in their extensive study of bulk Ni using a fully real-space DFT SD-PsP implementation. Last, we show another pseudopotential calculation employing norm-conserving PsPs.[24] We see that the LSDA yields the usual outcomes associated with overbinding: lattice constants that are too small and bulk moduli that are overestimated. As a result, although the lattice parameters given by all the norm-conserving potentials (SN-PsP and SD-PsP) are close to the experimental value, they fail to reproduce the AE value, which the PsPs are meant to reproduce. The values given for the bulk modulus are slightly underestimated (compared to AE results) for all PsPs, although our SD-PSP improves upon the SN-PsPs. As expected, the significant improvement of the SD-PsP over the SN-PsP is in the prediction of the magnetic moment per atom, where the use of the SD-PsP nicely corrects the problems due to the spin-neutral pseudopotential, yielding a magnetic moment per atom near to the AE value.

B. Bulk iron

The magnetic and structural properties of bulk iron provide a significant challenge to theory. First, there are inherent difficulties due to the type of exchange-correlation functional used. It is well known that the LSDA predicts the wrong ground-state crystal structure for Fe.[23,25] Second, several different magnetic and nonmagnetic phases exist, increasing the chances of seeing the pseudopotentials fail at correctly reproducing those phases. As a severe test of the capabilities of our spin-dependent pseudopotentials, we focus on the study of the cubic phases of Fe, using both the LSDA and the spin-polarized GGA-PBE approximation to the exchange-correlation potential.

1. LSDA results

Table V displays the LSDA bulk properties (lattice constant a_0, bulk moduli B_0, and magnetic moment per atom M) for the ferromagnetic bcc phase of Fe. LSDA calculations predict its energy to be higher than nonmagnetic fcc and hcp phases, despite the fact that the observed ground state is ferromagnetic bcc. Nevertheless, this failure of the

TABLE VI. DFT-LSDA structural energy differences (in eV/atom) between the ferromagnetic (FM) bcc phases of Fe and the nonmagnetic (NM) bcc and fcc phases.

	FLAPW[a]	SN-PsP	SD-PsP	US-PsP	SN-PsP	SD-PsP	US-PsP
NLCC	n/a	no	no	no	yes	yes	yes
$E_{\mathrm{bcc}}^{\mathrm{NM}}-E_{\mathrm{bcc}}^{\mathrm{FM}}$	0.29	2.03	0.13	2.53	0.35	0.35	0.26
$E_{\mathrm{fcc}}^{\mathrm{NM}}-E_{\mathrm{bcc}}^{\mathrm{FM}}$	−0.055	0.170	−0.020	0.216	0.001	0.001	−0.010

[a]Reference 30.

LSDA to correctly predict the ground-state properties of Fe affects equally AE and PSP methods, so our comparison between both is still valid. We again show results using the norm-conserving spin-neutral (SN-PsP) and spin-dependent (SD-PsP) pseudopotentials and an ultrasoft pseudopotential (US-PsP). We did two sets of calculations, with and without including a NLCC. When no NLCC is employed, both the SN-PsP and US-PsP give qualitatively similar results. For example, the lattice constant is significantly overestimated, contrary to the expectation that the LSDA should overbind and thus underestimate its value. The bulk modulus in both cases is greatly underestimated—lower or equal to the experimental one—when LSDA is expected to overestimate its value. The ferromagnetism of the cell is in both cases also quite poorly described, with up to 60% error in the magnetic moment per atom. When the spin-dependent pseudopotential is employed, the improvement is dramatic. Even though the lattice constant is slightly overestimated when compared to FLAPW results (by $\sim 2\%$), the SD-PsP value is smaller than the experimental one, obeying the typical tendency of LSDA to overbind, as is seen in the FLAPW results. For the bulk modulus, the value predicted by the SD-PsP is in excellent agreement with the AE one, and the improvement of the treatment of the cell magnetism is rather dramatic as well, with almost perfect agreement with AE results. When a NLCC is used, the results for the SN-PsP show an enhanced transferability of the pseudopotential, nicely correcting the obvious lack of accuracy of the pseudopotential without a NLCC. While the lattice constant and magnetic moment are much closer to AE values, the bulk modulus is improved but still is less accurate than with the SD-PsP. When the SD-PsP is used with a NLCC, the enhancement of transferability compared to the SN-PsP with NLCC is not as dramatic as before. Both a_0 and M are very similar to the SN-PsP with NLCC values, with the only real improvement being the evaluation of the bulk modulus B_0. It is quite surprising at first to see that the SD-PsP does not significantly improve the results over the SN-PsP when used with a NLCC, and even worse, the SD-PsP without a NLCC seems to give more satisfactory results than with a NLCC. We address this point in detail later, giving a rationale to explain this phenomenon. For the US-PsP, the improvement due to the use of NLCC is quite remarkable as well, exhibiting very good agreement with AE values for a_0 and M, even if the considerable overestimation of the bulk modulus can call into question its transferability.

Table VI shows the structural energy differences between the ferromagnetic (FM) bcc phase and the nonmagnetic (NM) bcc and fcc phases, within the LSDA approximation. Those results confirm the trends that were seen in Table V. Namely, when a NLCC is not applied, both SN-PsP and US-PsP behave extremely poorly: dramatically overestimating the energy splitting between the NM bcc and FM bcc phases and between the NM fcc and FM bcc phases, and even worse, yielding the wrong relative ordering for the latter. The use of the SD-PsP once again nicely corrects those inaccuracies, giving a slightly underestimated energy splitting for the NM bcc and FM bcc phases, and the correct relative ordering for the NM fcc and FM bcc phases, even though the energy difference is somewhat underestimated. When a NLCC is used, as in Table VI, we have enhancement of the transferability of the potentials, where all three SN-PsP, US-PsP, and SD-PsP give reasonable results compared to the AE FLAPW, although both SN-PsP and SD-PsP are not quite able to resolve the degeneracy between the NM fcc and FM bcc phases. Last, we again see that when a NLCC is used, the SD-PsP does not give as dramatic an improvement over the SN-PsP as it does when no NLCC is employed.

The special case of the fcc phase, with its inherent magnetovolume complexity, reveals even more dramatically the failure of the conventional spin-neutral pseudopotential method. Within the LSDA, the fcc phase has been shown from AE calculations to present a complex potential energy surface, where the lowest-energy fcc phase is seen to be nonmagnetic at low volume, but ferromagnetic ordering was shown to stabilize the phase at higher volumes.[25] Figure 1 shows the relative ordering between the NM and FM fcc phases as computed by our SN-PsP and SD-PsP, clearly showing the failure of the spin-neutral potential to correctly

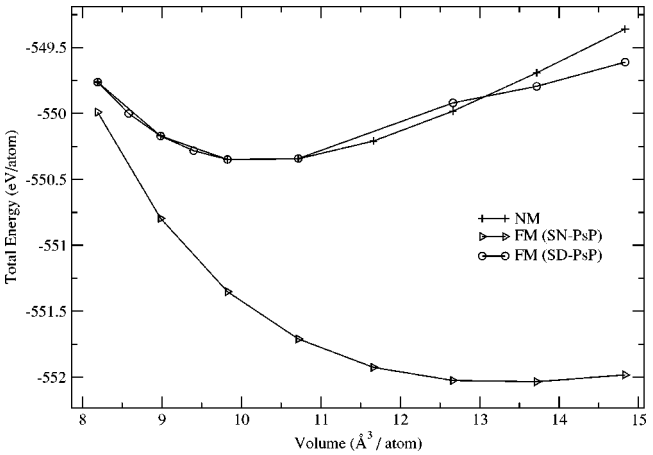

FIG. 1. fcc iron nonmagnetic (NM) and ferromagnetic (FM) phase ordering as predicted by DFT-LSDA calculations by a spin-neutral (SN-PsP) and spin-dependent (SD-PsP) pseudopotential.

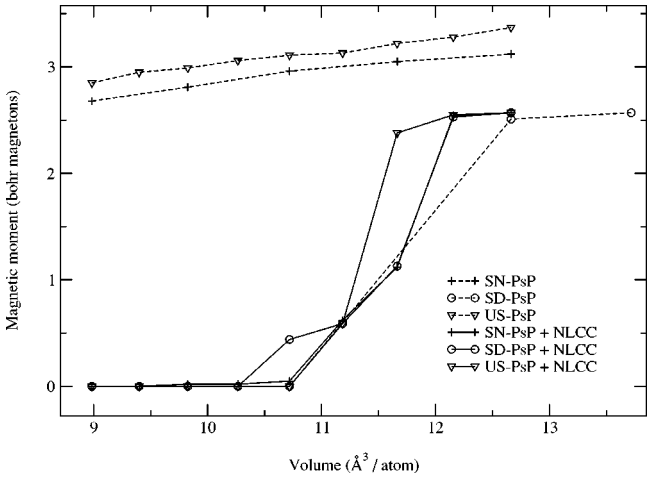

FIG. 2. Net magnetic moment vs volume for the fcc phase of Fe as calculated by several LDSA pseudopotential methods.

describe the complexity of the potential energy surface. The spin-neutral PsPs without a NLCC (i.e., the norm-conserving SN-PsP and the ultrasoft US-PsP) both yield two very distinct NM and FM phases, with the FM one being much lower in energy. Those potentials thus predict a very stable FM fcc phase and no branching with the NM phase. As for the spin-dependent potential, the correction is quite impressive, where we are able to resolve the magnetovolume effect, reflecting the degeneracy of both NM and FM phases at low volume, with branching as we increase the lattice parameter, just as in the AE calculations. Figure 2 provides a more complete illustration, showing the variation of the net magnetic moment per atom of the fcc unit cell as a function of cell volume for all our different pseudopotential methods. Both the SN-PsP and US-PsP without a NLCC give magnetic moments per atom that are far too large. When the SD-PsP is employed, we can see branching of the FM phase off the NM phase as the cell volume increases, followed by the persistence of ferromagnetic order up to $2.6\mu_b$, just as predicted by AE calculations. The use of a NLCC again greatly improves upon the PsP transferability, and all three methods give qualitatively similar results, in fairly good agreement with AE ones.

2. GGA results

Since the LSDA has been shown to fail in correctly predicting the ground-state properties of $3d$ transition elements,[23] we sought to apply our new spin-dependent pseudopotential formalism within a higher level of theory. This section discusses properties of different magnetic phases of cubic Fe using the GGA-PBE exchange-correlation functional.[22] As mentioned earlier, the use of a NLCC turned out to be required numerically in the case of gradient-corrected functionals in order to produce smooth and reliable pseudopotentials. Unfortunately, we did not have access to any ultrasoft potential for use with the GGA-PBE exchange-correlation potential, which would have provided a direct point of comparison.

Table VII shows the spin-polarized GGA-PBE results for the ferromagnetic bcc ground state of Fe as given by an AE

TABLE VII. GGA bulk properties of bcc Fe: lattice constant a_0, bulk modulus B_0, and magnetic moment per atom, M. All pseudopotentials include a NLCC.

	a_{latt} (Å)	B_0 (GPa)	M (μ_B)
Experiment	2.87	167	2.20
FLAPW[a] (PW91)	2.84	174	2.17
SN-PsP (PBE)	2.94	130	2.61
SD-PsP (PBE)	2.93	127	2.55
US-PsP[b] (PW91)	2.86	157	2.32

[a]Reference 26.
[b]Reference 7.

FLAPW calculation,[26] a spin-neutral pseudopotential (SN-PsP), and a spin-dependent PsP (SD-PsP). For comparison, we also include results reported earlier using an ultrasoft potential (US-PsP).[7] All pseudopotentials include a NLCC, although the formulation used for the US-PsP is different than ours. Because the PBE exchange-correlation potential is essentially a recast of the PW91 potential and since the errors introduced by the pseudopotential approximation in this case are expected to be much greater than the discrepancy between those two exchange-correlation potentials, it should not be a problem to compare directly results from PW91 (for FLAPW and US-PsP) with our PBE results (for SN-PsP and SD-PsP). The SN-PsP and SD-PsP both slightly overestimate the lattice constant compared to the AE value. Often, GGAs overcompensate for the errors in the LDA, thereby tending to underbind, which leads to overestimated lattice parameters. This occurs in our pseudopotential calculations but for some reason not in the AE FLAPW or the US-PsP calculations. We also underestimate the value of B_0 and overestimate the magnetic moment. Beyond the lack of transferability of the reference potential, the use of the SD-PsP improves only slightly on transferability, e.g., tending to reduce the overestimation of the ferromagnetic ordering. Figure 3 shows the GGA-PBE phase diagram of NM and FM cubic phases (bcc and fcc) of Fe. For the FM phases, both spin-neutral and spin-dependent pseudopotential results are shown. As expected from the use of GGA, FM bcc is now correctly pre-

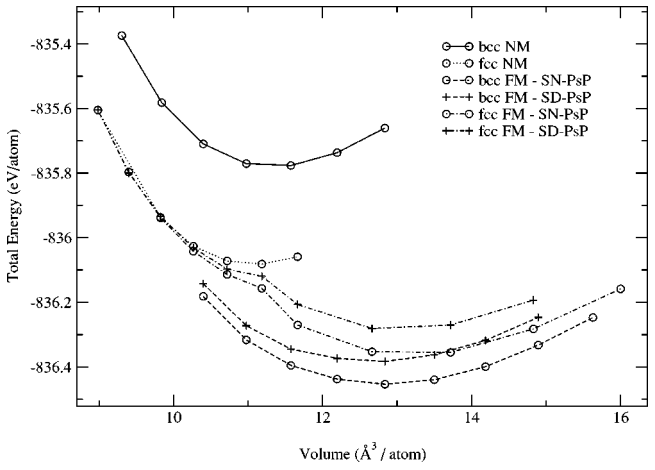

FIG. 3. DFT-GGA (PBE) phase diagram for the cubic phases of bulk Fe as predicted by our spin-neutral (SN-PsP) and spin-dependent (SD-PsP) pseudopotentials.

TABLE VIII. Spin-polarized GGA energy splittings between the NM and FM bcc phases of Fe and between the FM bcc and NM fcc phases of Fe.

Method	XC type	$E_{\mathrm{bcc}}^{\mathrm{FM}}-E_{\mathrm{fcc}}^{\mathrm{NM}}$	$E_{\mathrm{bcc}}^{\mathrm{NM}}-E_{\mathrm{bcc}}^{\mathrm{FM}}$
AE LMTO[a]	PW91	−0.14	0.43
SN-PsP	PBE	−0.37	0.67
SD-PsP	PBE	−0.29	0.59
US-PsP[b]	PW91	−0.24	0.56

[a]Reference 31.
[b]Reference 7.

dicted as the ground state, lying slightly lower in energy than the FM fcc phase after its branching away from the NM fcc phase. Qualitatively, both SN-PsP and SD-PsP seem to give similar results, although their associated energies, and thus the phase stabilities, are different.

Table VIII shows the structural energy differences between magnetic and nonmagnetic phases of bulk Fe. In all cases, the pseudopotential methods tend to overestimate those energy splittings, most dramatically in the case of the SN-PsP. Nevertheless, the SD-PsP corrects this tendency, and even provides results of fairly equal quality to the highly accurate US-PsP results published by Moroni *et al.*[7]

A preliminary conclusion is that the spin-dependent PsPs clearly tend to enhance the transferability of the usual spin-neutral PsPs in all respects. However, as discussed earlier, this improvement does not seem to be as dramatic when a NLCC is used. Evidently, the use of a NLCC already enhances the PsPs transferability, so that part of the ''job'' is already done. However, this answer is not entirely satisfactory. In fact, our LSDA results for bcc Fe showed that we were able to obtain better results using the SD-PsP without a NLCC than with, and it appears that the use of a NLCC was quenching the effects of the spin-dependence. Qualitatively, the SD-PsPs are based on a perturbationlike theory, and we saw that it essentially consists of giving the pseudopotential an extra degree of freedom (or self-adaptation) following its local chemical environment: depending on the local spin polarization around the atomic site, the pseudopotential adapts itself to a more (represented by the fully polarized potential v^{fp}) or less (by the spin-neutral reference v_0) polarized potential. When no NLCC is used, the discrepancy between those two atomic potentials is fairly large and the magnitude of the spin-dependent perturbation appreciable. However, when one uses a NLCC, the improved transferability makes those two atomic potentials more similar, thus diminishing the magnitude of the spin-dependent perturbation and the possible improvement gleaned from its use. To test our method in a more extreme case, we decided to apply our SD-PsPs to bulk Cr.

C. Bulk Cr

From both experimental and theoretical points of view, the properties of solid Cr are puzzling. It is generally understood that its ground state is a bcc phase showing a spin density wave (SDW) of about 20–21 lattice periods.[27] As far as DFT calculations are concerned, the study and understanding of the magnetic ground state of bcc Cr is still very much an area of active research.[28,29] Our goal is not to compare our work to the previous extensive work on the subject. Here we limit our study to the simpler antiferromagnetic (AF) phase of bcc Cr, which can be seen as an approximation to the real SDW. All-electron DFT calculations have shown that it is unclear whether LSDA or GGA is better for describing AF Cr.[28] The LSDA predicts a NM bcc ground state, with subsequent branching to the AF phase at larger volume, while the GGA predicts the branching to occur prior to the minimum in the potential energy curve, thereby predicting the correct ground state, AF bcc Cr.[28] But despite its inability to predict the correct structural properties, the LSDA seems to give a good description of the bulk antiferromagnetism, while the GGA dramatically overestimates it. The case of Cr is difficult even for an AE method, let alone for a pseudopotential technique. It may be necessary to include semicore p states as explicit valence states in order to obtain somewhat reasonable results. Spin-neutral PsPs are also expected to have difficulties at reproducing atomic orbital energies and bulk magnetism since Cr atom has a fully polarized electronic configuration (high-spin s^1d^5). We have generated two sets of potentials: one LSDA (SN-PsP and SD-PsP) and one GGA-PBE (SN-PsP and SD-PsP) where in all cases we included a NLCC. The semicore p states were left as core states, which comes with a penalty in terms of the transferability of the PsPs, but once again our goal is not to compare our results against experiment, but rather to monitor the systematic changes and/or improvements due to the spin dependence compared to a spin-neutral potential. As a consequence of not treating the semi-core p electrons explicitly, the use of a NLCC was necessary to generate a somewhat reasonably accurate spin-neutral reference potential.

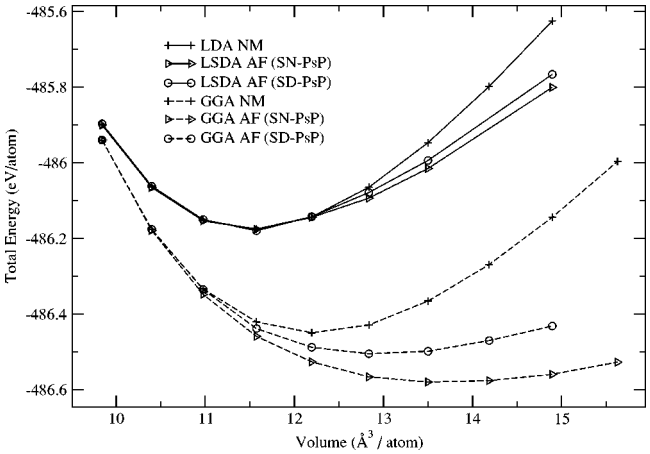

FIG. 4. Branching of the NM and AF phases of bcc Cr as calculated by spin-polarized LDA and GGA-PBE methods using a spin-neutral (SN-PsP) and a spin-dependent (SD-PsP) pseudopotential. All pseudopotentials include a NLCC. The GGA curves were uniformly shifted by 10.3 eV.

Figure 4 shows qualitatively the branching between the NM and AF bcc phases as a function of volume, as predicted by our PsP methods for both LSDA and GGA exchange-correlation potentials. As can be seen and in accordance with previous AE calculations, LSDA predicts a nonmagnetic ground state for bcc Cr, while GGA correctly gives an AF

TABLE IX. Spin-polarized DFT predictions of bulk properties for NM and AF bcc Cr: lattice constant a_0, bulk modulus B_0, and magnetic moment per atom, M. All pseudopotential calculations include a NLCC.

Method	Theory	a_0 (NM)	a_0 (AF)	B_0 (NM)	B_0 (AF)	M (a_0^{expt})[a]	M (a_0^{theo})[b]
Experiment (SDW)	n/a	n/a	2.88	n/a	191	0.62	n/a
FLAPW[c]	LSDA	2.79	n/a	308	n/a	0.63	n/a
SN-PsP	LSDA	2.85	n/a	305	n/a	0.17	n/a
SD-PsP	LSDA	2.85	n/a	305	n/a	0.30	n/a
FLAPW[d]	PBE	2.85	2.87	260	184	1.16	1.08
SN-PsP	PBE	2.90	3.00	257	71	1.87	2.62
SD-PsP	PBE	2.90	2.95	257	121	1.29	1.88

[a]Magnetic moment per atom at the experimental lattice parameter.
[b]Magnetic moment per atom at the computed lattice parameter.
[c]Reference 28.
[d]Reference 28.

ground state with lattice constant slightly larger than for the NM phase.

More detailed results are collected in Table IX. The LSDA results show that our pseudopotential does a reasonable job of reproducing AE values for the NM phase. The bulk modulus is in excellent agreement, with only the lattice constant being slightly overestimated in comparison to FLAPW results. As for the magnetic phase, our PsPs predict the branching between NM and AF phases to occur too ''late,'' leading to an underestimated net magnetic moment per atom at the shorter experimental lattice constant. While both pseudopotentials poorly reproduce the AE magnetic moment, the SD-PsP error is significantly less than the SN-PsP error. As in the case of the LSDA, our GGA PsP yields a bulk modulus that agrees well with the AE value for the NM phase, while slightly overestimating the equilibrium lattice constant. The main failures of the SN-PsP are found for the bulk modulus, where the result is far too low, while the values for the magnetic moment per atom at the experimental and theoretical equilibrium lattice constants are far too high. When the spin-dependent PsP is employed, the errors are significantly smaller in all properties calculated. In particular, while the bulk modulus is still underestimated, it is significantly improved over the SN-PsP, and the values of the magnetic moment are now in much better agreement with the AE ones. At the experimental lattice constant, the SD-PsP gives a very satisfactory magnetic moment and a much improved value for the magnetic moment at the theoretical lattice parameter. For both SN-PsP and SD-PsP, this lattice parameter is larger than the experimental one, which is not the case for the FLAPW one. Since cell magnetization always increases with volume expansion, it is thus normal that our PsPs give a magnetic moment at a_0^{theo} larger than the one at a_0^{expt}. The SD-PsP also gives a much more reasonable energy splitting between the NM and AF phases: FLAPW predicts the AF phase to be lower by 0.01 eV/atom, while the SN-PsP predicts the AF state to be lower by 0.13 eV/atom. When the SD-PsP is employed, this energy splitting is found to be 0.05 eV/atom, a significant improvement.

V. CONCLUSIONS

The properties of transition elements present great challenges for the pseudopotential approximation because of the difficulty of uniquely defining and generating pseudopotentials transferable enough for reliable use. It has become common practice to adjust the pseudopotential parameters to fit the desired results, which represents not only an unsatisfactory method for a so-called ''first-principles'' theory, but also does not guarantee an overall better transferability—a pseudopotential may very well work for some test cases and dramatically fail for others. The introduction of Vanderbilt's soft potentials allowed the cost involved with *d* elements to be dramatically reduced, but did not directly address the transferability question.

In this study, we have focused on the latter issue, where we have tried to make a fair comparison between the accuracy and transferability of the different pseudopotential methods, whenever possible, and to compare them against the new spin-dependent pseudopotentials that we have successfully implemented and applied in a reciprocal-space plane-wave code. Overall results show that US-PsPs, not surprisingly, do not show substantial improvement of the pseudopotential transferability over the more expensive norm-conserving ones. On the other hand, the use of a NLCC fixes some of the PSP's inaccuracies. Regarding our new method, the results for bulk Ni, Fe, and Cr show that the use of SD-PsPs improves the pseudopotential transferability in all instances. For the critical case of bulk Fe, we obtained accurate results and energetics without the use of a NLCC, where the SN-PsP's (norm-conserving or ultrasoft) invariably failed. When a NLCC is used, or must be used, the improvement is less dramatic but still sensible. We attribute this effect to the enhanced transferability due to the use of a NLCC that quenches the perturbative part added in our spin-dependent scheme. But the study of a fully polarized element like Cr clearly shows that even with a NLCC, there remains discrepancies between the spin-neutral and fully polarized pseudopotentials, and our results for bulk Cr suggest that, in fact, the use of the SD-PsPs can provide a significant improvement of PsP transferability beyond the use of a NLCC. But even though the question of pseudopotential transferability is essential from a qualitative point of view, the computational cost involved with norm-conserving potentials cannot be ignored, and therefore an ultrasoft formulation of the SD-PsP method is currently being developed. Combined with the computational advantages of the ultrasoft pseudopo-

tentials, the new SD-PsPs may provide an accurate and efficient pseudopotential method for the study of condensed phase magnetic materials, surfaces, interfaces, and other cases where an AE method becomes prohibitively expensive. Further study and comparisons against experiment are still needed to clearly assess the advantages of the method; this work is ongoing. For example, cases exist where no known pseudopotential has been able to reproduce all-electron results. These will be the focus of our future work to establish whether the SD-PsP can resolve such cases.

ACKNOWLEDGMENTS

The authors would like to thank Dr. Niranjan Govind for helpful discussions. We are also grateful to Dr. Martins for providing us with Froyen's atomic code. The code CASTEP is distributed by Accelrys Inc., San Diego, CA. This work has been funded in part by the NSF and the Army Research Office.

[1] W. E. Pickett, Comput. Phys. Rep. **9**, 115 (1989).
[2] N. Troullier and J. L. Martins, Phys. Rev. B **43**, 1993 (1991).
[3] I. Grinberg, N. J. Ramer, and A. M. Rappe, Phys. Rev. B **63**, 201102 (2001).
[4] D. R. Hamann, M. Schlüter, and C. Chiang, Phys. Rev. Lett. **43**, 1494 (1979).
[5] D. Vanderbilt, Phys. Rev. B **41**, 7892 (1990).
[6] A. M. Rappe, K. M. Rabe, E. Kaxiras, and J. D. Joannopoulos, Phys. Rev. B **41**, 1227 (1990).
[7] E. G. Moroni, G. Kresse, J. Hafner, and J. Furthmuller, Phys. Rev. B **56**, 15 629 (1997).
[8] K. Laasonen, R. Car, C. Lee, and D. Vanderbilt, Phys. Rev. B **43**, 6796 (1991).
[9] W. Kohn and L. J. Sham, Phys. Rev. **140**, A1133 (1965).
[10] S. G. Louie, S. Froyen, and M. L. Cohen, Phys. Rev. B **26**, 1738 (1982).
[11] D. Porezag, M. R. Pederson, and A. Y. Liu, Phys. Rev. B **60**, 14 132 (1999).
[12] D. M. Bylander and L. Kleinman, Phys. Rev. B **50**, 1363 (1994).
[13] S. C. Watson and E. A. Carter, Phys. Rev. B **58**, R13 309 (1998).
[14] F. Starrost, H. Kim, S. C. Watson, E. Kaxiras, and E. A. Carter, Phys. Rev. B **64**, 235105 (2001).
[15] L. Kleinman and D. M. Bylander, Phys. Rev. Lett. **48**, 1425 (1982).
[16] X. Gonze, R. Stumpf, and M. Scheffler, Phys. Rev. B **44**, 8503 (1991).
[17] M. Teter, Phys. Rev. B **48**, 5031 (1993).
[18] R. D. King-Smith, M. C. Payne, and J. S. Lin, Phys. Rev. B **44**, 13 063 (1991).
[19] M. C. Payne, M. P. Teter, D. C. Allan, T. A. Arias, and J. D. Joannopoulos, Rev. Mod. Phys. **64**, 1045 (1992).
[20] D. M. Ceperley and B. J. Alder, Phys. Rev. Lett. **45**, 566 (1980).
[21] J. P. Perdew and A. Zunger, Phys. Rev. B **23**, 5048 (1981).
[22] J. P. Perdew, K. Burke, and M. Ernzerhof, Phys. Rev. Lett. **77**, 3865 (1996).
[23] M. Asato, A. Settels, T. Hoshino, T. Asada, S. Blügel, R. Zeller, and P. H. Dederichs, Phys. Rev. B **60**, 5202 (1999).
[24] J.-H. Cho and M.-H. Kang, Phys. Rev. B **52**, 9159 (1995).
[25] J.-H. Cho and M. Scheffler, Phys. Rev. B **53**, 10 685 (1996).
[26] H. C. Herper, E. Hoffmann, and P. Entel, Phys. Rev. B **60**, 3839 (1999).
[27] V. L. Moruzzi and P. M. Marcus, Phys. Rev. B **46**, 3171 (1992).
[28] S. Cottenier, B. D. Vries, J. Meersschaut, and M. Rots, J. Phys.: Condens. Matter **14**, 3275 (2002).
[29] R. Hafner, D. Spisak, R. Lorenz, and J. Hafner, J. Phys.: Condens. Matter **13**, 239 (2001).
[30] C. Wang, B. Klein, and H. Krakauer, Phys. Rev. Lett. **54**, 1852 (1985).
[31] B. Barbiellini, E. Moroni, and T. Jarlborg, J. Phys.: Condens. Matter **2**, 7597 (1990).